Available online at www.sciencedirect.com
SCIENCE DIRECT®
Journal of Power Sources 129 (2004) 45–54
JOURNAL OF POWER SOURCES
www.elsevier.com/locate/jpowsour

High energy density strategies: from hydride-forming materials research to battery integration

P.H.L. Notten [a,b,*], M. Ouwerkerk [b], H. van Hal [b], D. Beelen [b], W. Keur [b], J. Zhou [a], H. Feil [b]

[a] *Eindhoven University of Technology, Den Dolech 2, 5600 MB Eindhoven, The Netherlands*
[b] *Philips Research Laboratories, Prof. Holstlaan 4, 5656 AA Eindhoven, The Netherlands*

Abstract

Two different strategies are outlined to develop both high energy density and space-efficient batteries, including the most widely applied rechargeable nickel-metal hydride (NiMH) and Li-ion batteries. The hydrogen storage capacity of fluorite-structured Mg-containing compounds are shown to have a reversible electrochemical storage capacity of more than four times that of the commonly used MischMetal-based AB_5 compounds in NiMH, i.e. 1500 mAh/g (5.6 wt.%). The formation of octahedral sites within the crystal lattice is argued to be very crucial for the improved kinetics of hydrogen absorption and desorption. It is shown that the fluorite-structure can be conserved with both precious Sc and the less expensive Ti up to a Mg content of 80 at.%. Both thermodynamic and kinetic data are presented in relation to the materials composition. In addition, the development of preshaped batteries, as the first step to battery integration, has contributed to a much higher level of design freedom for portable electronic equipment. The manufacturing process of preshaped batteries will be described together with their electrochemical characteristics. Advantageously, the mechanical stability is provided locally by polymer rivets, allowing to get rid of heavy metallic casings and to make use of a much wider range of battery shapes.

Keywords: Hydrogen storage; Hydride-forming compounds; NiMH batteries; Preshaped batteries; Li-ion; Freedom of design

1. Introduction

The use of portable electronic equipment has been rapidly growing during the last two decades. This has, on the one hand, been accomplished by the strong development of microelectronics and, on the other hand, by the successful introduction of high energy density rechargeable batteries, such as nickel-metal hydride (NiMH) [1–3] and Li-ion [4,5]. NiMH is reported to have a more than 50% higher volumetric and gravimetric energy density than conventional NiCd batteries whereas, in particular, the gravimetric energy density for Li-ion has been improved even further, making this latter system very attractive for portable applications [6]. Despite the fact that there is an ongoing tendency towards miniaturisation, resulting in a significant power reduction this is, however, counterbalanced by the strong trend towards more build-in functionality of portable equipment. For example, the introduction of full-colour displays and various video applications in portable phones are power-consuming features. Consequently, at present the power consumption is significantly overruling the power reduction, clearly indicating that a further increase of the energy density of rechargeable batteries is not only a desire but a necessity.

Another aspect, which is becoming very important, is the freedom of the design for portable electronic products. This design is experienced to be one of the leading selling points, distinguishing products from competing manufacturers. However, it is nowadays common use that the design is adapted towards the shape of commercially available batteries. Since nowadays mainly cylindrical and rectangular shaped cells are available in the market this put some serious limitations to the freedom of product design. We, therefore, considered another, rather unconventional, approach: explore the possibility to adjust the battery shape towards the electronic end product.

Several strategies can be adopted to further increase the energy density of rechargeable batteries. Developing new materials and battery integration are evidently interesting options. In this paper we will focus on both aspects: one part will be devoted to the development of new dense, hydride-forming, materials to be applied in NiMH batteries and possibly as hydrogen storage material in fuel cells [7–9] and the other part will be related to the development of so-called preshaped Li-ion-based batteries [10,11].

* Corresponding author.
E-mail address: peter.notten@philips.com (P.H.L. Notten).

0378-7753/$ – see front matter © 2003 Elsevier B.V. All rights reserved.
doi:10.1016/j.jpowsour.2003.11.019

In order to compete with the high gravimetric energy density of present-day Li-ion batteries new, light-weight, hydride-forming materials are under development at our laboratory, which can store more than four times the hydrogen content than the $LaNi_5$-type hydride-forming compounds nowadays widely applied in commercial NiMH batteries. Based on our "switchable mirror" research [12,13], Mg-based compounds were found to reveal a very high and electrochemically reversible hydrogen content [14,15]. In contrast to the frequently investigated Mg-compounds these compounds do have a more favourable crystallographic fluorite-structure enhancing the kinetics significantly. Electrochemical and crystallographic results of these materials will be presented.

Another way to increase the energy storage efficiency is not to take the batteries as starting point but to start with the (portable) electronic equipment, which have to be powered. Very often the shape and hence the design of portable electronic equipment, is "dictated" by the shape of the batteries or battery packs. A lot more freedom of design can be obtained when the shape of the batteries is adapted to that of the equipment. With this in mind we have recently developed so-called "preshaped" batteries. Based on conventional Li-ion technology, the Lithylene rivet technology has been developed [10,11], which can, on the one hand, be used to produce very flat, large area, batteries and, on the other hand, to manufacture curved batteries, which perfectly fit into the housing of electronic equipment, cars, etc. The principles of this new approach will be outlined and demonstration models will be shown.

2. Experimental

2.1. Hydrogen storage materials

All catalyst-doped Sc-containing materials were prepared from the melt by mixing the appropriate amounts of starting elements under purified argon and subsequently annealing the samples inside a Mo-crucible for 4 days at 450 °C [16]. The Ti-containing materials, on the other hand, were prepared by ball milling the individual hydrides under a controlled hydrogen atmosphere (7 bar). Details about various aspects of the materials preparation will be reported in a separate paper [17].

Powders were obtained by crushing and filing the Sc-materials. Obviously, powdered materials were directly obtained in the case of the Ti-materials. All materials were characterised by conventional techniques like XRD, scanning electron microscope (SEM), electron probe micro analyses (EPMA), to investigate their homogeneity, phase-formation/separation, etc. [16]. Only the powders that passed through a 50 μm sieve were used for the electrochemical experiments. Electrodes were made in our standardised way [3,18] by mixing the Mg-based powders with either Ni or Ag powder in the ratio of 1 to 5, respectively, and pressing the powders under controlled conditions into pellets. Ag is sometimes used because it has a substantial larger stability window than Ni [19].

All electrodes were tested in conventional thermostated three-electrode cells [3] containing 6 M KOH. Conventional electrochemical experiments, including galvanic interruption titration technique (GITT), were performed at 25 °C and using an Hg/HgO (6 M KOH) reference electrode. All electrode potentials in alkaline electrolytes refer to this reference.

2.2. Preshaped batteries

The developed Lithylene technology can be applied to both flat and preshaped Li-ion batteries. The advantage of this technology is that it can simply make use of existing, commercially available, materials. In the present work we used commercial electrodes, separators and electrolytes, nowadays widely applied in Li-ion technologies, i.e. conventional graphite anodes, separator (Celgard) and $LiCoO_2$ cathodes [10]. Since the technology is stack-based both single-sided (ss) electrodes and double-sided (ds) electrodes are applied to the exterior and interior of the battery stack, respectively. The electrodes are either mechanically or laser cut. Prior to the electrode assembly small holes with diameter of 0.95 and 1.25 mm for the anode and cathode, respectively, are either punched or laser cut. The distance between the rectangular positioned holes are, in this example, 5 mm [11]. Both the diameter and the repeating distance are not fully optimised but the stack integrity appeared to be very good for the chosen dimensions.

Heating the applied polymer forms an integer stack after which the stack is packed into a polymer-coated Al foil. Subsequently, the stack is impregnated with a conventional electrolyte (1.0 M $LiPF_6$ in EC/DEC/DMC (40:20:40 wt.%)). The details how preshaped batteries are constructed will be further outlined in the results section (see also Ref. [11]).

After battery preparation the cells were formed for at least three cycles by the conventional low-current constant-current–constant-voltage (CCCV) charging and CC discharging. The electrochemical characteristics were also determined by applying conventional CCCV-charging and CC-discharging. CCCV consisted of 0.2 C-rate charging till 4.2 V and CV charging continues till the current had dropped to 0.05 C. After a resting period of 30 min, the batteries were discharged at 0.2 C till the cut-off voltage of 3 V was reached. The rate-capability tests were performed using the above standard charging and varying discharging conditions at room temperature. In order to obtain a well-defined starting condition the batteries were additionally discharged with a low-current in all cases (0.2 C). The cycle-life tests were performed by (dis)charging with 0.5 C. To get information about the total available capacity, the (dis)charging current was decreased to 0.2 C every tenth cycle.

3. Results and discussion

3.1. Hydrogen storage materials

A typical galvanostatic charging and discharging experiment of an $Mg_{0.8}Sc_{0.2}Pd_{0.024}$ electrode, inside an Ag-matrix, is shown in Fig. 1A. Charging is performed at a relatively high rate of 250 mA/g. Two regions can be distinguished in charging curve (a), the first one at a potential of about −1.1 V at which water reduction is accompanied by hydride-formation, according to:

$$H_2O + e^- \leftrightarrow H_{ad} + OH^- \quad (1)$$

$$H_{ad} \leftrightarrow H_{abs} \quad (2)$$

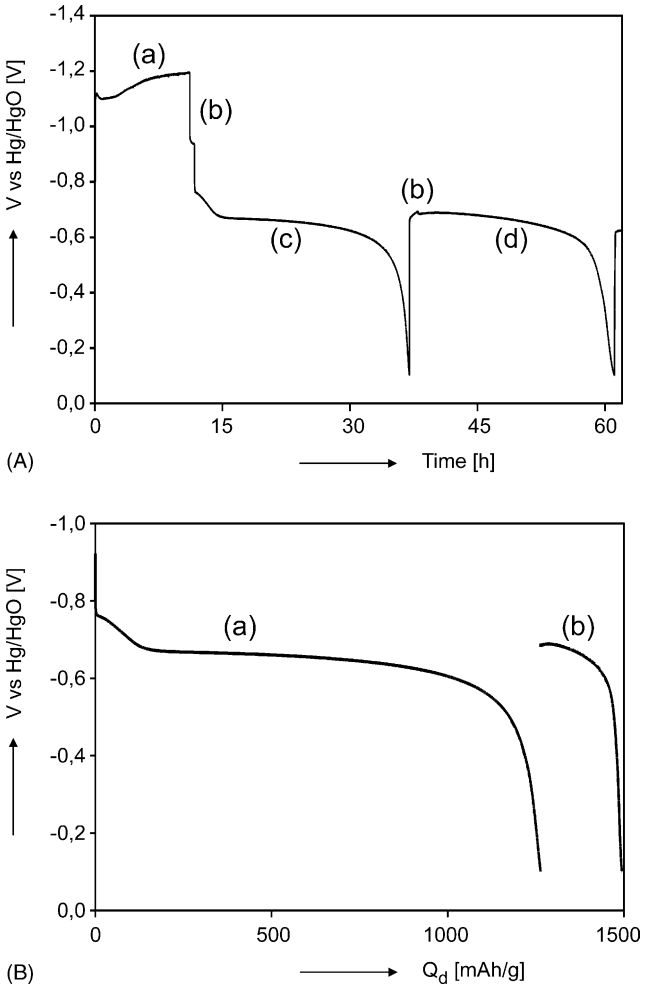

Fig. 1. Typical galvanostatic electrode cycle of an $Mg_{0.8}Sc_{0.2}Pd_{0.024}$ electrode (A). Constant-current (250 mA/g) charging (a) is followed by a resting period (b) of 30 min allowing the electrode to relax to the equilibrium state before a constant discharge current (50 mA/g) is commenced (c). After the cut-off voltage of −0.1 V is reached the electrode is put under open-circuit condition again (b). Subsequently, deep-discharging with 10 mA/g is initiated (d). (B) Voltage discharge curves vs. the amount of extracted charge.

followed by a second plateau region where hydrogen atoms recombine to molecular hydrogen gas.

$$2H_{ad} \leftrightarrow H_2(g) \quad (3)$$

This latter plateau region indicates that the electrode is fully hydrogenated. After charging is completed the electrode is allowed to relax towards the open-circuit period (curve b). An open-circuit potential of about −926 mV indicates that the partial hydrogen pressure is close to 1 bar [3]. Subsequently, the electrode is discharged with 50 mA/g (curve c). After the cut-off voltage of −0.1 V has been reached the electrode is again put at rest (curve b). Additional low-current deep-discharging (10 mA/g) allows the electrode to release some extra amount of hydrogen (curve d).

In Fig. 1B the same results are plotted as a function of the released amount of electrical charge (Q_d). It is important to note that the major part of the hydrogen is already oxidised during the high-current discharge period (curve a). Some 15% of the stored hydrogen is additionally removed at the lower discharge rate (curve b), most likely due to transport limitations. The total amount of reversibly discharged hydrogen (Q_d) amounts to 1500 mAh/g hydride-forming material. This corresponds to reversible hydrogen content of $H_{1.73}$ or 5.6 wt.%! It should, however, be noted that, even under these low-current conditions, not all hydrogen could be released from the electrode. A small part of hydrogen is so tightly bonded to the crystal lattice that it cannot be removed under these ambient conditions. This has been reported before for other hydride-forming rare-earth materials [12,20] and the present Mg-based compounds [9].

It has been argued before that the presence of a highly electrocatalytic material such as Pd is extremely important to drive the electrochemical charge transfer reaction. This holds for both thin film and bulk materials [3,12]. It has been reported that the discharge capacity of the present materials decreases dramatically when the Pd-content is lowered. Our results indicate that substantial gain can be reached by further optimising with respect to both catalyst content and catalyst distribution.

The influence of the materials composition on the high-current (50 mA/g) discharge capacity is shown in Fig. 2. Obviously, the discharge capacity increases dramatically with increasing Mg-content. Two voltage regions can be clearly distinguished in the discharge plots. During the initial stages of the discharge process a sloping plateau region can be discerned. The extent of this sloping region is clearly dependent on the Sc-amount: the smaller the Sc-content the smaller this region. Furthermore, the voltage level is higher for the Sc-rich materials. Whether this is related to thermodynamic or kinetic aspect cannot be concluded from these experiments. The second voltage plateau region is typical for a phase separation process, which is often found in electrochemical hydride-formation/decomposition reactions [3,21,22]. Strikingly, the voltage level of these plateaux is almost independent on the materials composition, indicating that

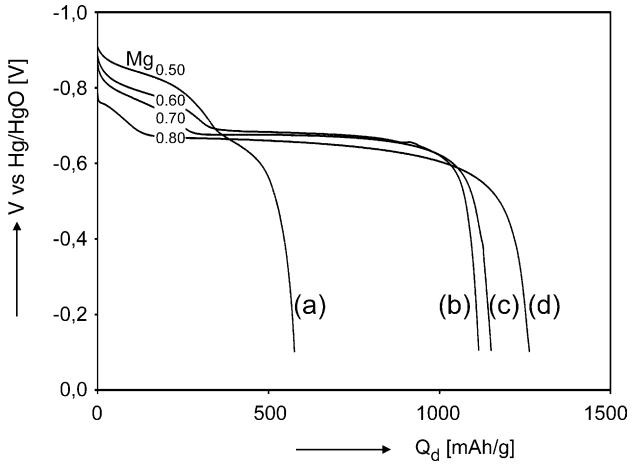

Fig. 2. Voltage discharge curves resulting from constant-current (50 mA/g) discharging electrodes with varying composition $Mg_xSc_{1-x}Pd_{0.024}$. The Mg content (x) was varied in the range of 0.5 and 0.8; 0.5 (a); 0.6 (b); 0.7 (c) and 0.8 (d).

irrespective of the composition the partial hydrogen pressure is more or less fixed.

Fig. 3 shows the dependence of Q_d on the materials composition obtained after high-rate (50 mA/g) discharging (curve a) and additionally low-rate (10 mA/g) discharging (curve b). In agreement with Figs. 1 and 2 the discharged capacity increases with increasing Mg-content. A maximum of 1500 mAh/g is reached for $Mg_{0.8}Sc_{0.2}Pd_{0.024}$. It has been analysed by means of XRD that materials with an Mg-content in the range of $0 \leq Mg \leq 0.8$ have a cubic, fluorite-structure [9]. When the Mg-content goes beyond this maximum the kinetics of the hydride decomposition reaction decreases dramatically to very low Q_d values for pure Mg. Strikingly, in line with this observation the crystallographic structure was found to change from fluorite to the Mg-familiar rutile-structure (Fig. 3). The kinetics

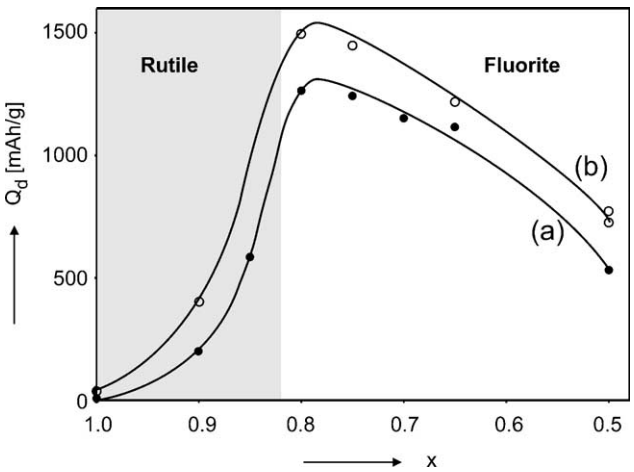

Fig. 3. Discharge (a) and deep-discharge (b) capacities (Q_d) for electrodes with varying composition $Mg_xSc_{1-x}Pd_{0.024}$ with Mg content (x), ranging from $0.5 \leq x \leq 1$. The crystallographic regions as derived from XRD are also indicated.

of conventional Mg-based materials is indeed reported to be extremely poor and is generally considered as one of the most problematic limitations of the commonly investigated Mg-based compounds [23]. It has been argued that, the present fluorite-structures are one of the key factors to ensure favourable hydrogenation kinetics [9].

Both the thermodynamics and kinetics of the various Mg compounds have been investigated by GITT. After a pulse charging period the electrode were allowed to equilibrate. The dependences of the equilibrium voltage on the level of discharging are shown in Fig. 4A. The results are very close to the results obtained under current flowing conditions as shown in Fig. 2. Again a sloping, compositional, dependent region can be distinguished during the initial stages of discharging at high hydrogen content, subsequently, followed by a flat, two-phase, plateau region. Adopting the well-known relationship between the equilibrium voltage (E^{eq}_{MH}) and the partial hydrogen pressure (P_{H_2}),

$$E^{eq}_{MH} = -0.926 - \frac{RT}{nF} \ln \frac{P_{H_2}}{P_{ref}} \quad (4)$$

a plateau pressure of the order of 10^{-6} to 10^{-7} bar can be calculated where P_{ref} refers to $P_{ref} = 1$ bar $\approx 10^5$ Pa [3]. This value is in good agreement to what is expected for pure Mg-hydride at room temperature [24].

The results of Fig. 4A suggests that the voltage plateau region is due to the complete dehydrogenation of MgH_2 whereas during the initial stages of the discharge process the Sc-trihydride compound is only partly converted into Sc-dihydride. Adopting this simple reaction scheme yields the following equation for the reversible hydrogen storage for the present, fluorite-structured Mg-based compounds:

$$Mg_xSc_{1-x}H_{2(1-x)} + (x+1)H_2O + (x+1)e^- \leftrightarrow Mg_xSc_{1-x}H_{3-x} + (x+1)OH^- \quad (5)$$

For the sake of simplicity we herewith assume that the Pd-hydride does not significantly contribute to overall storage capacity and is, therefore, left out of Eq. (5). The total discharge capacities found in the fluorite region (Fig. 3) are in fair agreement with such elementary model. A reversible hydrogen storage capacity of $H_{1.73}$ for $Mg_{0.8}Sc_{0.2}Pd_{0.024}$ is indeed, according to Eq. (5), close to what is expected for $x+1$ (=1.8). It is furthermore to be expected that a decrease of the Mg-content reduces the storage capacity, as indeed is found in Fig. 3.

Fig. 3 shows that the hydrogen kinetics at/inside the fluorite structure is much more favourable than the rutile structure. Hydrogen can occupy both tetrahedral and octahedral sites in these fluorite-based materials. The octahedral sites are argued to be essential for this favourable transportation mechanism and are promoted by the introduction of trivalent metals, like Sc [8,9]. During the discharge process the hydrogen located at the octahedral sites are thought to be removed first (see structure of fully charged electrode in Fig. 4A). Interstitial tetrahedral bounded hydrogen would then become

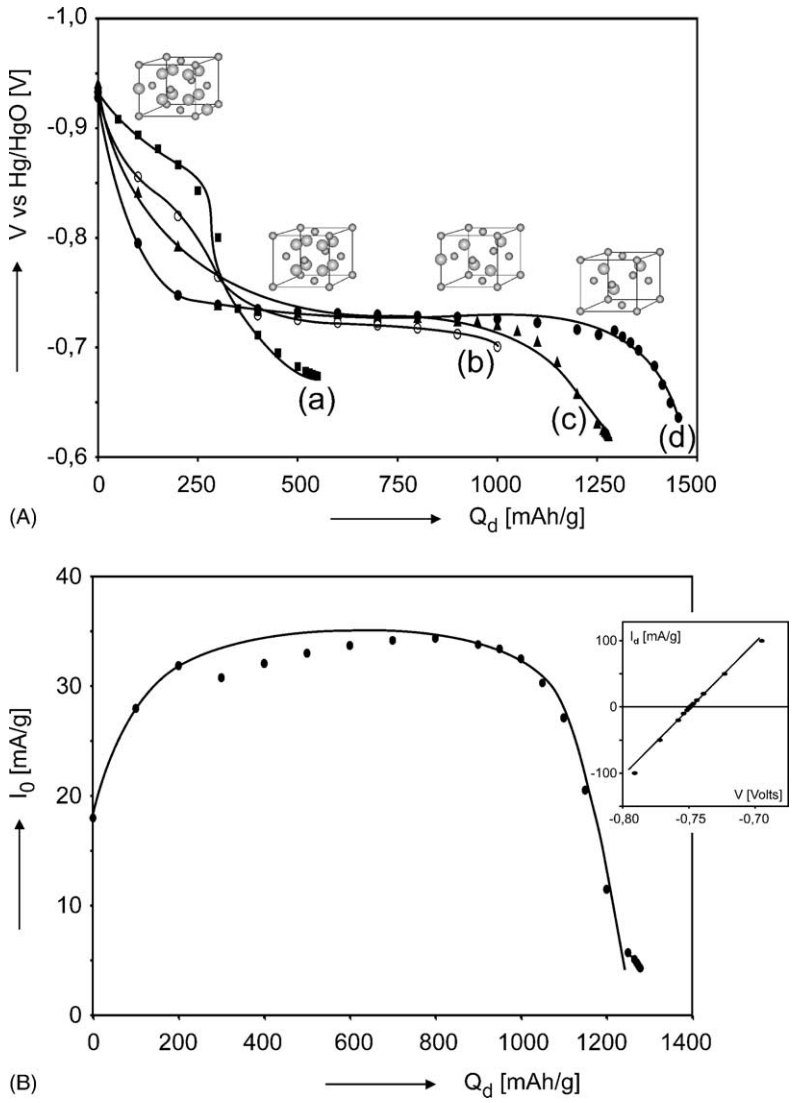

Fig. 4. Equilibrium voltage curves obtained during GITT discharging experiments (A) at 25 °C for $Mg_xSc_{1-x}Pd_{0.024}$ containing electrodes with $0.5 \leq x \leq 0.8$; 0.5 (a), 0.6 (b), 0.7 (c) and 0.8 (d). The crystallographic changes induced by the discharging process and measured by ex situ XRD are indicated for the high capacity $Mg_{0.8}Sc_{0.2}Pd_{0.024}$ material. (B) Dependence of the exchange current (I_o) on the electrochemical discharge level (Q_d). The inset shows a typical current/voltage measurement from which I_o has been calculated.

highly mobile by hopping along the large empty octahedral sites within the structure. Following the discharge curve, part of the tetrahedral sites is subsequently discharged.

In addition, the exchange current was measured at each equilibrium open-circuit voltage along the GITT experiment. The result shown in Fig. 4B, reveals a bell-shaped curve. This is in line with the mathematical considerations described before [3,25]. Comparing these I_o measurements with those reported before for $LaNi_5$-type compounds indicates that the charge transfer kinetics of the present Mg-based compounds is still about a factor of 6 lower [18]. It should, however, be noted that for the present Mg-compounds the catalyst distribution has not been optimised yet, as was clear from microscopic investigations [9,16]. On the other hand exchange current measurements at rutile-structured Mg-compounds were found to be extremely low. The good kinetic results do not give, however, a full understanding of the improved transport properties. Both optimisation and more detailed transportation measurements are in progress.

In conclusion, Fig. 5 shows a comparison of the high-rate discharge behaviour of a conventional AB_5-type electrode with that of the present fluorite-structured $Mg_{0.72}Sc_{0.28}(Pd_{0.012}Rh_{0.012})$ electrode. In this compound the Pd-catalyst has been replaced by a mixture of PdRh, which turned out to be more beneficial. Evidently, the gravimetric storage capacity has been increased by more than a factor of 4, indicating that the hydrogen storage capacity has been increased from about 1.2 to 5.6 wt.%. It should, however, be noted that the electrochemical cycle-life

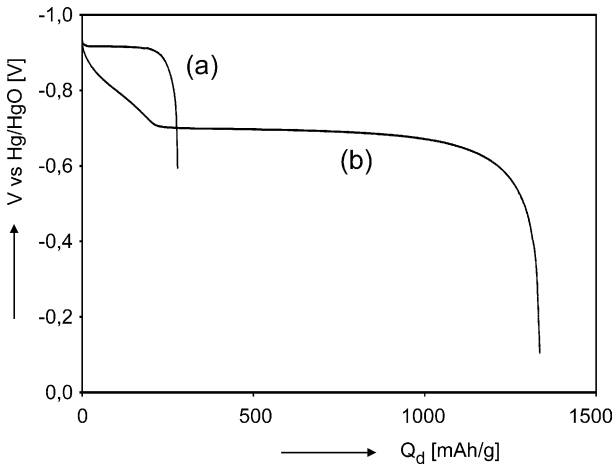

Fig. 5. Comparison of the galvanostatic (50 mA) discharge curves for a conventional AB_5-type electrode material (a) and the newly developed Mg-based $Mg_{0.72}Sc_{0.28}$ ($Pd_{0.012}Rh_{0.012}$) compound (b).

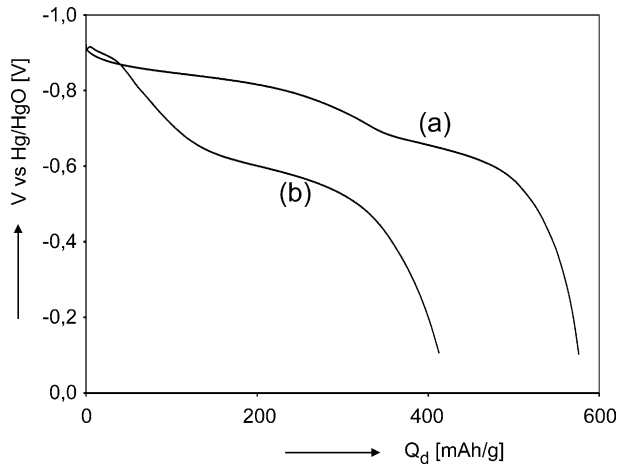

Fig. 6. Comparison of the galvanostatic (50 mA/g) discharge curves for not yet optimised, Mg-based, Sc-containing $Mg_{0.5}Sc_{0.5}Pd_{0.024}$ (a) and Ti-containing $Mg_{0.5}Ti_{0.5}Pd_{0.024}$ (b).

performance of the present materials is not yet optimised. For example, Sc-containing ($Mg_{0.65}Sc_{0.35}Pd_{0.05}$) electrodes are found to loose approximately 50% of its initial storage capacity after 50 full electrochemical charge and discharge cycles. The origin of this capacity loss has been investigated by means of EPMA and could be attributed to the oxidation of the hydride-forming electrode particles in the electrochemical environment, making the surface of these particles no longer active for hydrogen absorption. It should, however, be emphasised that the stability of gas-phase storage might be much better as the aggressive alkaline medium is then excluded. This latter issue might be of special

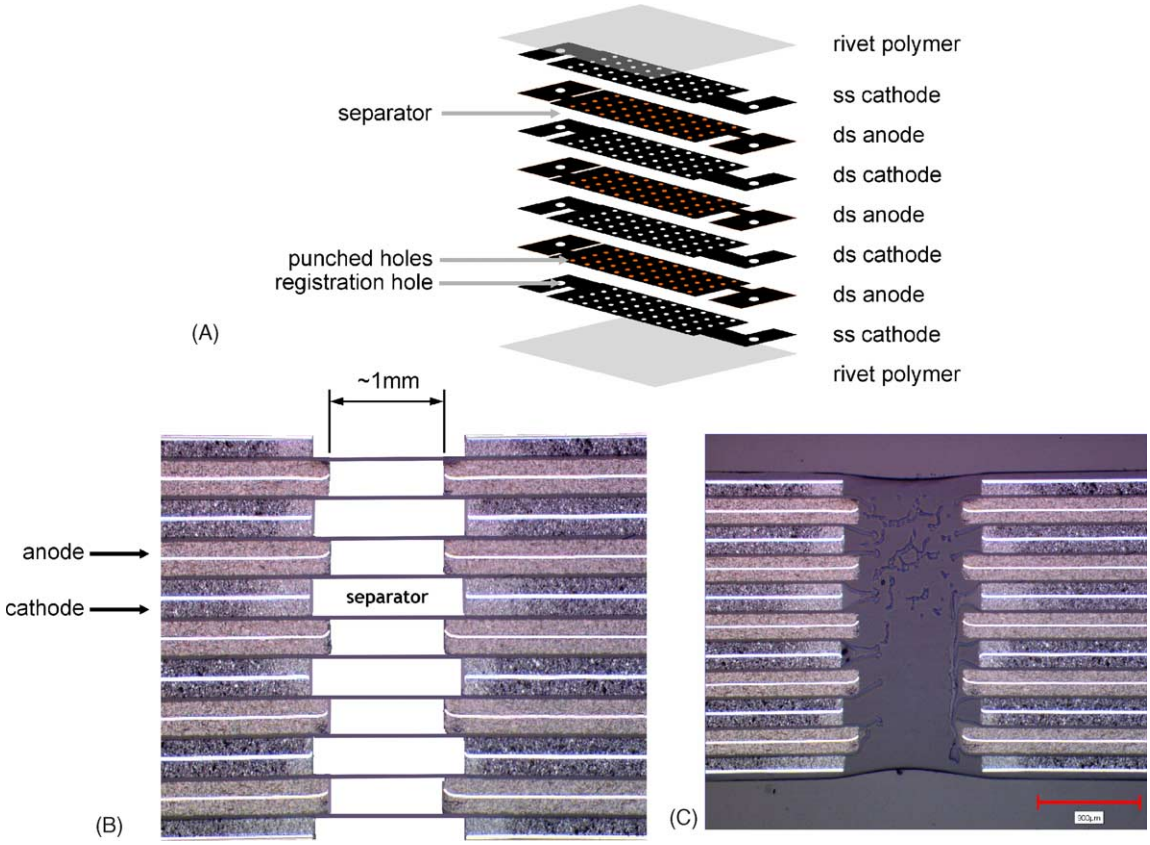

Fig. 7. Schematic representation of how a Lithylene battery is constructed (A). Optical microscopic cross-section of the stack prior to the annealing step (B) and just after annealing and subsequent cooling (C).

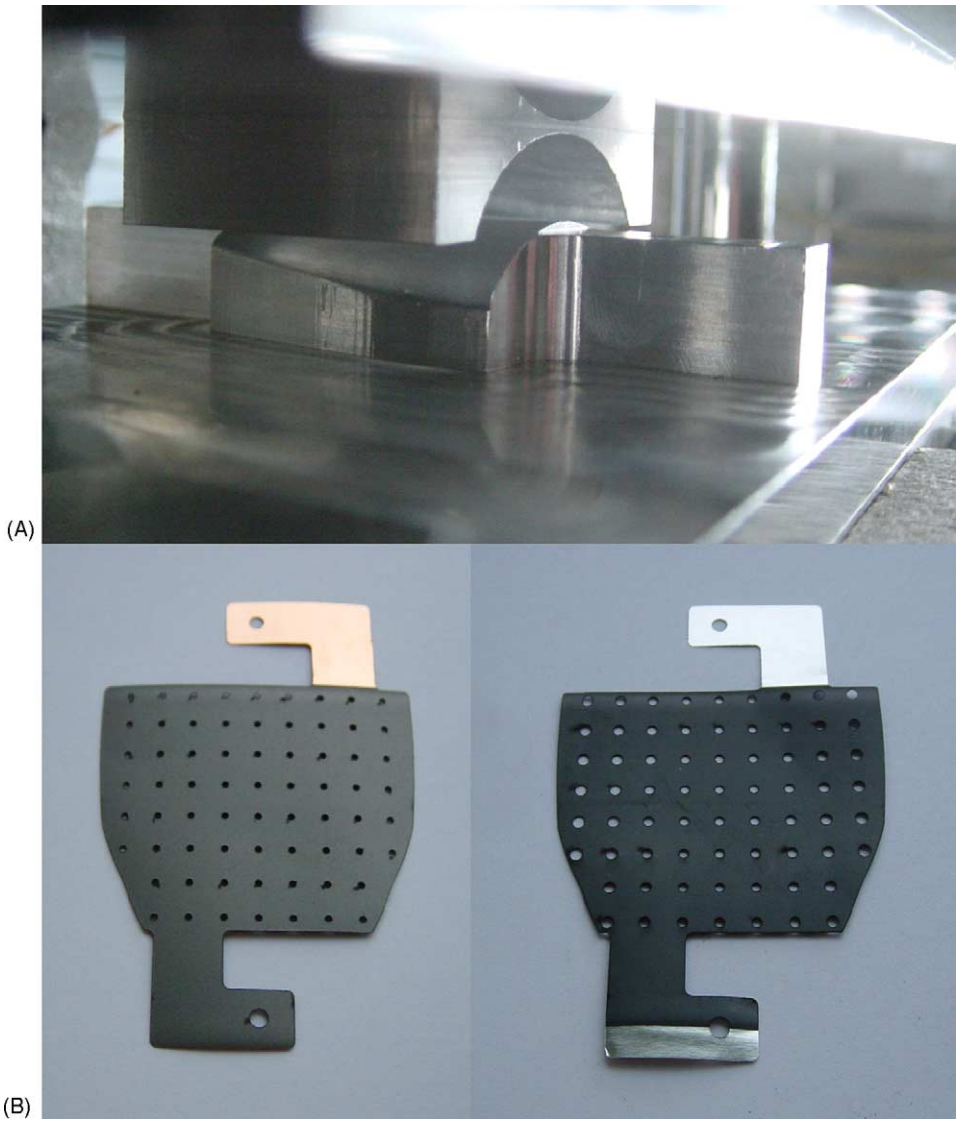

Fig. 8. Upper and lower parts of the preshaped riveting tools (A) and examples of flat and preshaped, laser-cut electrodes, clearly revealing the pattern of the 1 mm holes (B).

importance for storage applications related to fuel cells. The impact of the kinetic and corrosion properties in both electrochemical and gas-phase media will be subject for further investigations.

One drawback of the present materials is that both the noble catalysts and Sc are rather expensive. We, therefore, directed our research to replace the precious Sc by a more low-cost material while preserving the favourable fluorite-structure of the Mg-compounds. Fig. 6 shows a preliminary result of this investigation. It compares the result of an Sc-based and a Ti-based electrode material. Although it should be emphasised that this is one of the very first experimental attempts it is clear that the discharge curves of both compounds are very similar. In addition, XRD measurements showed that both compounds reveal the same fluorite structure. These results indicate that new ways have been opened to further explore the capabilities of this interesting class of Mg-based hydride-forming compounds.

3.2. Preshaped batteries

The principle of the Lithylene technology is schematically represented in Fig. 7A, revealing a stack of the individual components. A single-sided $LiCoO_2$ cathode forms the basis of the stack. A double-sided graphite anode is, subsequently, positioned on top of the cathode that is followed by a double-sided positive electrode. The stack can be then repeated, ending up with the final single-sided cathode and the rivet polymer sheet. As can be seen in Fig. 7A, each of these electrodes has already been punched with small holes. The required separators are placed in-between the positive and negative electrodes in order to prevent short circuit. A cross-section of the as-prepared stack is shown in

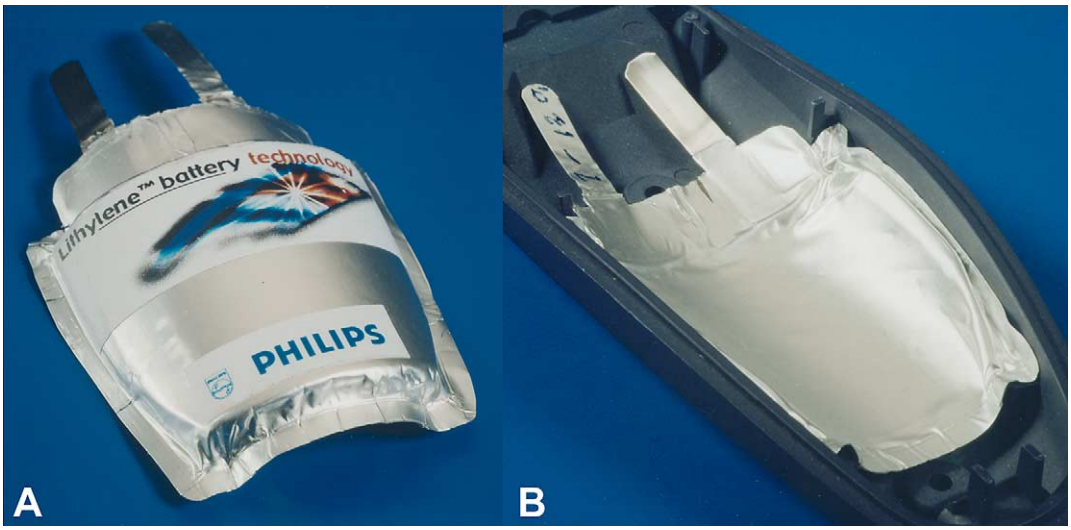

Fig. 9. Example of an as-prepared preshaped Li-ion battery (A) and the preshaped battery positioned inside the plastic housing of a portable, electronic, equipment (B). Note that the battery fits perfectly well inside the housing and that the radius of the battery is continuously changing.

Fig. 7B. Melting them with hot needles subsequently opens the separators locally bridging the holes. Afterwards, the stack together with the rivet polymer sheets that are applied to the exterior of both single-sided positive electrodes is placed in-between a hot press at 120 °C for 2.5 min. During this so-called riveting process, the polymer melts and penetrates each of the holes under the specified heating and pressure conditions. After cooling under pressure, the polymer hardens, keeping the cell's active materials together and providing a very mechanically stable battery structure. The cross-section after cooling is presented in Fig. 7C.

The most important character of this technology is that the stack can be preshaped during the riveting step. This can simply be achieved by using preshaped riveting tools (Fig. 8A) and, dependent on the shape of the battery, preshaped flat electrodes (Fig. 8B). After packaging into an impermeable polymer-coated Al foil, impregnation of the electrolyte and evacuation, the final step of the preparation procedure is sealing the battery. An example of an as-produced preshaped battery is shown in Fig. 9A. The radius of the battery is, in this example, continuously changing from 1.45 to 1.72 cm and, consequently, it fits perfectly well into the housing of a portable electronic device, as Fig. 9B reveals. In this way the scarce empty space inside the often small-sized electronic products can be utilised much more efficiently. Compared to conventional Li-ion batteries a higher specific energy density can be obtained with the present polymer rivet technology since the metallic cans, essential to maintain the mechanical integrity of these systems, can be replaced by locally operating polymer anchors.

A conventional CCCV (dis)charging cycle is shown in Fig. 10. Both the current and voltage responses are shown

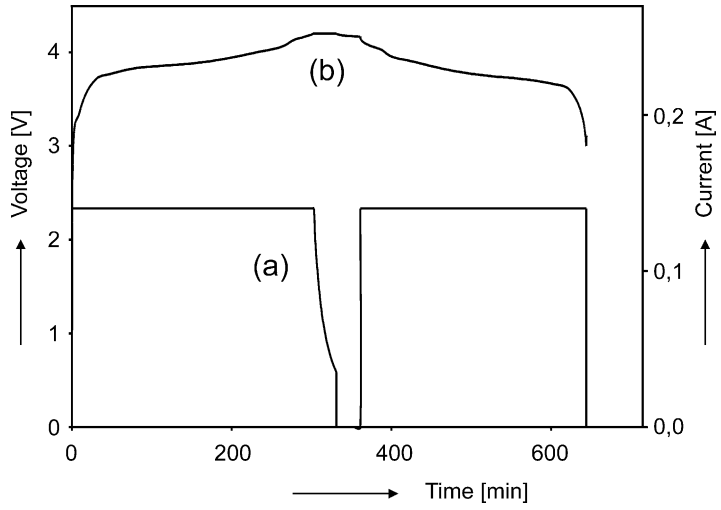

Fig. 10. Typical CCCV-charging and CC-discharging cycle applied to the 750 mAh preshaped battery shown in Fig. 9 at 25 °C. Apart from the current (*I*), curve (a), the resulting battery voltage (*V*), curve (b), is also indicated.

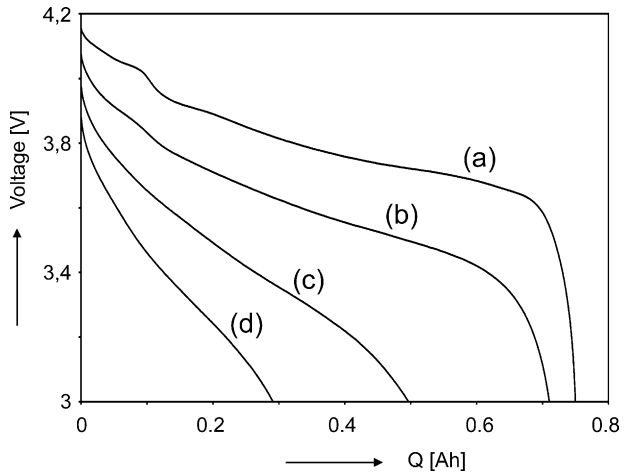

Fig. 11. Voltage discharge curves of a preshaped Li-ion battery (750 mAh) upon discharging at various loads at 25 °C: 0.2 C (a), 1 C (b), 2 C (c) and 3 C-rate (d). The standard charging conditions were the same in all cases.

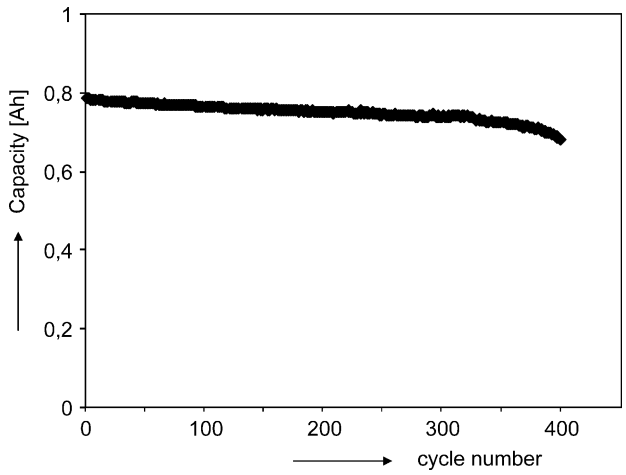

Fig. 12. Cycle-life experiment for a preshaped battery under standardised cycling conditions at 25 °C. The preshaped battery has a nominal capacity of 750 mAh.

and reveal that the result is very similar to what is normally found for conventional Li-ion batteries, as expected.

The results of rate-capability measurements are shown in Fig. 11. At a 0.2 C discharge rate (curve a), the battery delivers 750 mAh, which is in good agreement to what is expected on the basis of the theoretical capacity, and is therefore, to be considered as the nominal capacity of 100%. Discharging with 1 C the voltage drops and the battery delivers 95% of its nominal capacity (curve b), which is comparable to some commercial Li-ion batteries. The voltage decreases further and the discharge capacity drops more significant at a 2 and 3 C rate to 500 and 290 mAh, viz. 66 and 39% of the nominal capacity, respectively. Compared with some commercial Li-ion batteries, the discharge capacity of preshaped batteries at high C rate is relatively poor [26–28]. As mentioned before, all components, including the electrolyte employed in preshaped batteries are commercial materials. This means that the performance of the battery is, therefore, mainly controlled by the properties of the materials available in market. An additional advantage is that once new high energy density electrodes become available these quickly can be embraced by the present preshaped technology.

Fig. 12 presents the results of a cycle-life test of a preshaped battery at room temperature. The initial storage capacity is found to be close to 800 mAh and capacity decays gradually upon cycling. After 400 cycles the capacity is, however, still more than 85% of its initial storage capacity. It is well-known that the electrodes experience severe shrinkages and expansions upon cycling. This evidences that the polymer rivets are indeed able to supply a very good mechanical stability even under the long-term cycling conditions. We compared these electrochemical results of preshaped batteries with those obtained with flat Lithylene batteries and found that the results are more or less the same. The results are also in good agreement with those of commercial Li-ion batteries, as expected.

4. Conclusions

Two promising strategies to increase the energy density of batteries are reviewed. The first concept is based on the development of new lightweight hydrogen storage materials, which can be applied as storage materials in both rechargeable batteries and hydrogen driven fuel cells. In order to improve the hydrogen mobility in magnesium-hydride it has been successfully attempted to stabilise this compound in the fluorite-structure by partially substituting the magnesium with trivalent scandium or titanium. This has resulted in a very high reversible electrochemical storage capacity of up to 1500 mAh/g.

The second strategy is to adapt the shape of batteries to that of the design of the electronic product. This has resulted in the as-denoted preshaped batteries, which fit perfectly well into the housing of electronic products, delivering a high degree of design freedom. This interesting new technology is based on the Lithylene rivet technology, through which the mechanical strength of the electrode stack is supplied, replacing the metallic can in conventional Li-ion batteries. The preshaped Li-ion batteries reveal a high specific energy, and most importantly they offer a large degree of shape flexibility.

Acknowledgements

The authors would like to thank Mr. H. Wondergem for the materials XRD analyses.

References

[1] J.J.G. Willems, Philips J. Res. 39 (1984) 1.
[2] I. Matsumoto, M. Ikoma, 16th International Power Sources Symposium, Power Sources 12 (1988) 203.

[3] P.H.L. Notten, in: F. Grandjean, G.J. Long, K.H.J. Buschow (Eds.), Rechargeable nickel-metalhydride batteries: a successful new concept, NATO ASI Series E, vol. 281, London, 1994, Chapter 7, p. 151.
[4] T. Nagaura, in: S.P. Wolski (Org), International Symposium on Rechargable Battery Seminar, Paper 15, Deerfield Beach, FL, 1990.
[5] J.B. Goodenough, in: S.P. Wolski (Org), 19th International Seminar on Primary and Secondary Battery, Florida Educational Seminar, Fort Lauderdale, 2002.
[6] P.H.L. Notten, J.R.G. van Beek, Chem. Ind. 54 (2000) 102.
[7] M. Ouwerkerk, D. Beelen, H.A.M. van Hal, W.C. Keur, Extended Abstract No. 64, 202nd Electrochemical Society Meeting, Salt Lake City, 2002.
[8] M. Ouwerkerk, D. Beelen, H.V. Hal, W. Keur, P.H.L. Notten, Extenced Abstract No. 1261, 203nd Electrochemical Society Meeting, Paris, 2003.
[9] M. Ouwerkerk, D. Beelen, H. van Hal, W. Keur, P.H.L. Notten (2003) in preparation.
[10] http://www.lithylene.philips.com.
[11] J. Zhou, H. Feil, P.H.L. Notten (2003) in preparation.
[12] P.H.L. Notten, M. Kremers, R. Griessen, J. Electrochem. Soc. 143 (1996) 3348.
[13] R. Griessen, J.N. Huiberts, A.T.M. van Gogh, N.J. Koeman, J.P. Dekker, P.H.L. Notten, J. Alloys Compd. 253/254 (1997) 44–50.
[14] P. van der Sluis, M. Ouwerkerk, P.A. Duine, Appl. Phys. Lett. 70 (1997) 3356.
[15] P.H.L. Notten, Curr. Opin. Solid State Mater. Sci. 4 (1999) 5.
[16] D. Beelen, H.A.M. van Hal, W.C. Keur, M. Ouwerkerk, Extended Abstract No. 65, 202nd Electrochemical Society Meeting, Salt Lake City, 2002.
[17] D. Beelen et al. (2003) in preparation.
[18] P.H.L. Notten, P. Hokkeling, J. Electrochem. Soc. 138 (1991) 1877.
[19] R.A.H. Niessen (2003) private communications.
[20] P.H.L. Notten, Recent research developments in electrochemistry, Transworld Research Network, 3 (2000) 1 (ISBN 81-86846-66-2).
[21] T.B. Flanagen, W.A. Oates, Hydrogen in intermetallic compounds I, in: L. Schlapbach (Ed.), Topics in Applied Physics, Springer Verlag, New York. 63 (1988) 49.
[22] J.-M. Joubert, M. Latroche, A. Percheron-Guegan, MRS Bull. 27 (2002) 694.
[23] P. Selvam, B. Viswanathan, C.S. Swamy, V. Srinivasan, Int. J. Hydrogen Energy 11 (1986) 169.
[24] R.C. Bowman, B. Fultz, MRS Bull. 27 (2002) 688.
[25] P.H.L. Notten, A. Ledovskikh, M. Ouwerkerk, H. Senoh, C. Iwakura, J. Alloys Compd. 356–357 (2003) 759.
[26] D. Linden, T.B. Reddy (Eds.), Handbook of Batteries, McGraw-Hill, New York, 2002.
[27] P. Ramadass, B. Haran, R. White, B.N. Popov, J. Powers Sources 111 (2002) 210.
[28] D. Aurbach, B. Markovsky, A. Rodkin, M. Cojocaru, E. Levi, H.J. Kim, Electrochim. Acta 47 (2002) 1899.